ClinicSearch

Clinical Trials and Case Studies

Festus, Chioma *

Open Access

Research Article

Corrosion Inhibition and Antimicrobial Studies of Hydroxynaphtaldehyde Imine Chelator and its M(II) Chelates: Synthesis, Analytical, and Theoretical Characterizations

Festus, Chioma [1*], Wodi Theresa Chizoba [1] and Chioma D. Don-Lawson [2]

[1] Department of Chemistry, Ignatius Ajuru University of Education,P.M.B. 5047 Rumuolumeni, Port Harcourt, Rivers State, Nigeria.

[2] Department of Chemistry, Rivers State University, Port Harcourt, Nigeria.

***Correspondence Author:** Festus, Chioma, Department of Chemistry, Ignatius Ajuru University of Education,P.M.B. 5047 Rumuolumeni, Port Harcourt, Rivers State, Nigeria.

Received Date: January 27, 2023 | Accepted Date: February 03, 2023 | Published Date: February 10, 2023

Citation: Festus, Chioma. Corrosion Inhibition and Antimicrobial Studies of Hydroxynaphtaldehyde Imine Chelator and its M(II) Chelates: Synthesis, Analytical, and Theoretical Characterizations, *Clinical Trials and Case Studies*, 2(1); **DOI:**10.31579/2835-835X/011

Abstract

Organic molecules with some or all of their atoms connected in rings with at least one non-carbon atom, particularly from the nitrogen family, are common in many fields of life science and technology. They constitute the vast majority of the molecules involved in the operation of living creatures as well as in the man-made medications, herbicides, inhibitors, and fragrances used by man to exert control over nature. Thus, the synthesis and characterization; antimicrobial and corrosion inhibition (CI) studies; and DFT evaluations of some bivalent metal chelates from bidentate imine-chelator (LH) acquired through reflux condensation of 2-hydroxyl-1-naphthaldehyde and 2-amino-6-ethoxybenzothiazole reported in this current study. The antibacterial and antifungal properties of the synthesized compounds were tested *in-vitro* against *P. mirabilis, E. coli, S. aureus, K. oxytoca, S. Epidermidis, S. Pneumoniea, A. niger, A. flavus,* and *Fuserium Sp*. strains. The FTIR spectra of LH revealed a band at 1622cm^{-1}, which was ascribed to the azomethine function's(-C=N-) stretching vibration. This band appeared at lower frequencies in the M(II) chelate spectra, indicating chelation. The UV-Vis and magnetic susceptibility (µ*eff*) data of the chelates propose a 6-coordinate assemblage around the central ion except Ni(II) chelate which adopted tetrahedral geometry. The chelates displayed good thermal stability. Jobs method of continuous variation suggests 1:2 metal to ligand ratio. The effect of imine chelator, LH and its metal chelates on acid deterioration of mild steel (ms) could be visible from the result that the LH had considerable CI performance in contrast to corrosion of ms in a 1M HCl solution. Generally, the complexes exhibited enhanced antimicrobial activity against the microbes than the free chelator. The premeditated zinc complex had the best antibacterial activity while manganese complex showed enormously fine antifungal actions against the screened microbes with inhibitory zones of 15.0 and 26.5 mm separately.

Keywords: abdominal trauma; hemoperitoneum; pancreas trauma

Introduction

Schiff-based compounds are important and widely used for various functions due to their high thermal and moisture stability at different temperatures (Sadia et al., 2018). They are used as optical materials, polymers, dyes, pigments, steel/iron corrosion inhibitors, as well as for heavy metal spectral analysis and as catalysts in various related reactions to high temperatures (Tisato et al., 1994; Mesbah et al., 2018; Sadia et al., 2018). Schiff bases (SBs) have been used to produce novel chemotherapeutic compounds (Sadi et al., 2006) because many of them serve as models for biological species in the field of bio-inorganic (Debdulal, 2019). Many SB compounds exhibit remarkable catalytic activities owing to the presence of H_2O vapor (Xavier & Srividhya 2014). Recently, there has been renewed interest in SB complexes due to the search for drugs with better overall therapeutic effects while being less hazardous (Zhaohua et al., 2001). Due to the complexity involved in biological systems, the reactivity of these compounds has increased biologically and their inherent chemical benefits as polydentate chelators have promoted the increase in discovering their coordinated behavior (Jones et al., 2016).

The thiazole ring is important in nature due to its content. Penicillin, the first and foremost broad-spectrum antibiotic contains tetrahydrothiazole in its structure (Linda et al., 2021). Thiazole and thiazolamine are essential drugs (Thakar et al., 2011). Several biological activities are known to be conceivable for compounds with thiazole and 2-aminothiazole rings (Iswatun &Nurziana, 2021). In pharmacology, 2-aminothiazole derivatives are widely used. They also have antibacterial and antioxidant properties. Several aminothiazole substitutes are used as antioxidant additives in hydrocarbons, minerals and synthetic lubricants, as well as solid paraffins, polyolefins and vegetable fats (Mohamed et al.,

2021). Triazine derivatives with 2-aminothiazole moiety are active anti-scratch, anti-wear and anti-corrosion additives for lubricating oils. Rust, especially in humid atmospheres and acidic environments, is a major obstacle to the widespread use of ms in most industries, as it is widely used for structural purposes (Fayomi et al. al., 2021In general, industries use acids for pickling and cleaning of structural steel, and these processes are always complicated by significant metal decomposition (Fayomi et al., 2021). However, the use of inhibitors remains the most effective corrosion prevention technique (Prakash, 2019).

Organic compounds with heteroatoms in aromatic rings are often used as corrosion inhibitors. These compounds have the ability to adsorb onto metal surfaces and block active sites on the surface, thereby reducing the rate of corrosion. Many chelator-inhibitors have demonstrated good corrosion inhibitory properties at different temperatures in different acidic environments (Singh et al., 2020). The most effective corrosion inhibitors such as organic molecules with polar functional groups such as sulfur, oxygen and nitrogen have conjugated systems and hydrophobic components that help to protect metals from corrosive environments (Festus &Wodi 2021). Previously, our research group synthesized and investigated the CI potential of several 2-(thiazol-2-ylamino)-2,3-dihydonaphthalene-1-4-dione complexes (Chioma and Theresa, 2022). In this paper, we present the synthesis of SB formed by condensing 2-hydroxyl-1-naphthaldehyde with 2-amino-6-ethoxybenzothiazole, its complexation with transition elements and their antimicrobial and anti-corrosion activities.

Materials and Methods

Divalent acetate salts (Mn, Ni, Cu, Zn), sulfate (Fe) and chloride (Co), Zn-dust, 2-hydroxyl-1-naphthaldehyde (2-HNA), 2-amino-6-ethoxybenzothiazole (2-AEBT)), purchased from Aldrich Coy Germany. To document the infrared and electronic spectra of the compounds, the Perkin Elmer Spectrum-100 spectrometer with KBr plates and the PEKIN ELMER LAMBDA 25UV/VISIBLE spectrometer (190-900 nm) were used independently. The magnetic sensitivity of the synthesized chelates was investigated using the Festus and Don-Lawson's method (2018). The antibacterial and antifungal experiments were performed exactly as Festus et al., (2020).

Synthesis of the chelator and divalent chelates

The chelator (Figure 1) was prepared by dissolving 11.26g and 10.00g of 2-AEBT and 2-HNA in 30 mL ethanol solution. The resulting solution was refluxed for 6 hr with stirring. The resulting pale yellow precipitate was filtered and recrystallized with C_2H_5OH (Abel-Olaka et al., 2019). The imine-chelator bivalent metal chelates were synthesized by reacting calculated sum of the chelator (LH, 1.1 g, 1.58 x 10-3 mL) and the respective metal (0.387 g, 0.44 g, 0.375 g, 0.39 g, 0.32 g and 0.35 g of Mn(II), Fe(II) , Co(II), Ni(II), Cu(II) and Zn(II)) salts in 2:1 ratio according to a method published in the literature (Festus et al., 2020) (Figure 2). The resulting compounds were dried on anhydrous $CaCl_2$ (Gomathi and Selvameena, 2013).

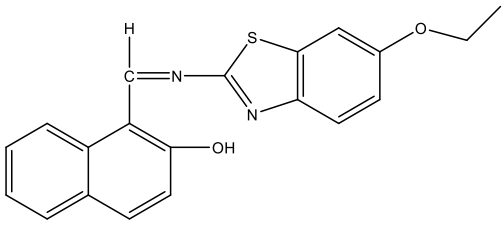

Scheme 1. Proposed structure of the Schiff base Ligand

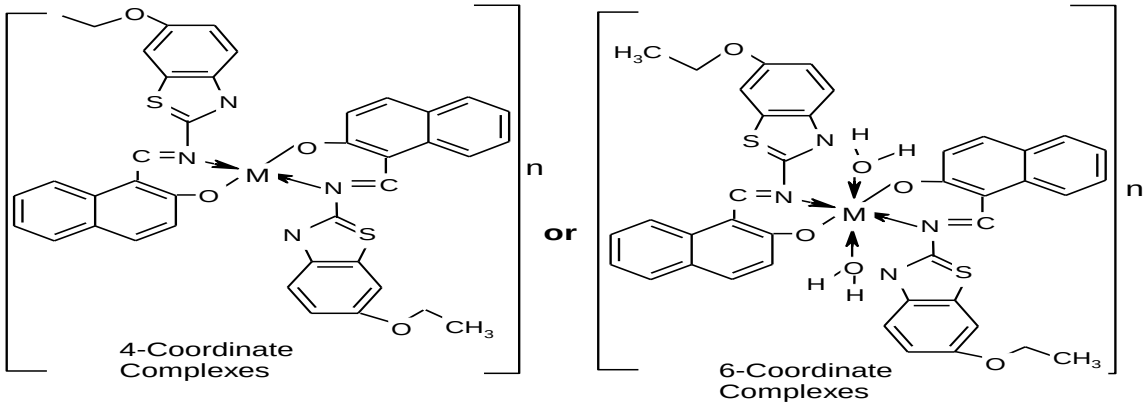

Scheme 2: Proposed structure of the metal (II) complexes

Ci Studies

Preparation of ms Coupons: The ms sheet obtained from Rivers State University with approximate compositions: C(0.120%), Mn($9.0x10^{-1}$ %), S($6.6x10^{-2}$ %), P($5x10^{-2}$ %), Si($1x10^{-1}$ %) and Fe(98.314%), of thickness 0.5 and 0.7mm was cut into rectangular coupons of dimensions 40/40 mm and 50/40 mm. The coupons were prepared following a literature method (Madueke and Iroha, 2018)

Gravimetric Measurements: A mole of HCl solution was prepared by diluting 37% HCl reagent grade with twofold distilled H_2O. For inhibition investigations, different amounts of inhibitor solutions were produced by dissolving the required amount of LH and its bivalent chelates in 50 mL of 1M HCl. A blank test solution of 100 mL of 1M HCl without the inhibitor was prepared. The weight loss experiment was carried out exactly as earlier described by Festus and Wodi (2021).

Results and Discussion

Physiochemical Data

The synthesized compounds were typically colored solids that were soluble in organic solvents but varied in their stability in air. Acquired data denotes that a molar ratio of 1:2 of M-L, which supports the

stoichiometry of the type $[M(L)_2]$ and $[M(L)_2(H_2O)_2]$ for the 4- and 6-coordinate chelates, respectively. The molar conductance values found in $(CH_3)_2SO$ were very low (9.3-37.2 $ohm^{-1}cm^2$) to allow complex dissociation and indicate the complexes' non-electrolytic character. Except for Zn(II) chelate, which was diamagnetic, the µ*eff* result indicated that other chelates were paramagnetic (Table 1). The µ*eff* values of the chelates at room temperature were also compatible with 6-coordinate assemblage, with the exception of Ni(II) chelate, which revealed tetrahedral geometry. The chelates had greater melting points than the parent imine chelator, indicating that they were more stable than the imine chelator.

Compounds	Molecular Weight	M. Pt(c°)/ Yield(%)	Shade	µ*eff* (BM)	Ohm^{-1} cm^2mol^{-1}
LH $C_{2o}H_{15}O_2N_2S$	347.01	180-183 /76	Yellow	-	-
$[Mn(L)_2(H_2O)_2]$ $MnC_{40}H_{34}O_6N_4S_2$	975.702	210-212 /51	Deep brown	6.81	09.3
$[Fe(L)_2(H_2O)_2]$ $FeC_{40}H_{34}O_6N_4S_2$	928.834	194-197 /70	Brown	6.77	28.7
$[Co(L)_2]H_2O$ $CoC_{40}H_{32}O_5N_4S_2$	968.542	245-247 /41	Dark brown	4.93	37.2
$[Ni(L)_2(H_2O)]$ $NiC_{40}H_{32}O_5N_4S_2$	979.462	239-242 /33	Oxy-blood brown	4.0	20.1
$[Cu(L)_2(H_2O)_2]$ $CuC_{40}H_{34}O_6N_4S_{22}$	937.104	230-232 /69	Light brown	2.2	33.9
$[Zn(L)_2(H_2O)_2]$ $ZnC_{40}H_{34}O_6N_4S_2$	986.124	280-283 /70	Orange	0.76	15.9

Table 1: The physicochemical data of the imine chelator and its M(II) chelates

FT-IR Spectra

Table 2 describes the stretching vibrations of the imine chelator, LH, and its chelates. With an absorption band at 1622 cm^{-1}, the infrared spectra of LH indicated the formation of imine bonds (-C=N-) and the lack of carbony1 bonds (C=O). The latter was present in the chelates as well, albeit at lower wavenumbers between 1616 and 1620 cm^{-1}, indicating the participation of the imine N-atom in coordinating with the M(II) ions (Festus, 2017). Similarly, at 1600-1602cm^{-1}, the stretching vibration of C=C groups was seen in the spectra of LH and its chelates. A broad absorption band at 3337cm^{-1} was ascribed to intra-molecular H-bonding vibration (vO-H), which was frequently observed in imine chelators containing hydroxyl groups (Sayed et al., 2020, Kpee et al., 2018). The detected OH bending vibration at 940 cm^{-1} in the chelator shifted to a higher wavenumber in the chelates, demonstrating the existence of H_2O molecules (Festus et al., 2021; Chioma et al., 2023). The weak absorption bands found in the chelates of $[Co(L)_2(H_2O)_2]$, $[Cu(L)_2(H_2O)_2]$, and $[Zn(L)_2(H_2O)_2]$were assigned to the (=C-H) aromatic stretching vibration, whereas the (C-H) aliphatic asymmetric stretching band was detected at 2926 cm^{-1} but moved to a higher wavenumber (2976-2978) cm^{-1} in the spectra of the chelates. Furthermore, C-O absorptions between 1057-1142 cm^{-1} suggest the existence of an alcohol/phenol group (Amani et al., 2018). A sharp but short intensity band at 1213-1264 cm^{-1} was designated to stretching vibration of N(C-N) automatic group (Sahar et al., 2021). This band shifted to emerge as a sharp albeit medium intensity band in the chelates' spectra between 813-834 cm^{-1} (Fengtao et al., 2018). The LH acted as an asymmetric bi-dentate chelator composed of N and O atoms from an amine and carbonyl moieties. Due to the participation of carbonyl O and deprotonated amine N atoms binding to the M(II) ions, two additional bands at 633-588 and 403-499 cm^{-1} formed in the far infrared portion of the complexes' spectra, indicating the establishment of metal to nitrogen (M-N) and metal to oxygen (M-O) bonds (Aliyu and Sani, 2012).

Compound	LH	$[Mn(L)_2(H_2O)_2]$	$[Fe(L)_2(H_2O)_2]$	$[Co(L)_2(H_2O)_2]$	$[Ni(L)_2(H_2O)]$	$[Cu(L)_2(H_2O)_2]$	$[Zn(L)_2(H_2O)_2]$
OH/H_2O	3337	3417	3433	3418	3420	3422	3425
-C=N	1622	1621	1622	1617	1620	1616	1618
-C=C	1601	1601	1602	1601	1602	1660	1601
Aromatic C-N	1232	1270	1232	1230	1213	1264	1231
Stretch C-O	1057	1142	1059	1058	1062	1066	1058
C-H Stretch	2926	2977	2978	2976	2925	2977	2976
Aliphatic C-C	1036	1058	1036	1041	1062	1042	1042
C-S	813	813	813	829	834	826	832
C-C Stretch (n ring)	1574	1574	1575	1576	1578	1573	1581
=C-H Aromatic	-	-	-	3059	-	3059	3041
CH rocking in plane	748	743	743	744	750	745	744
OH bending	942	942	964	975	979	984	974
=C-H aromatic bend	-	-	942	941	943	946	942
CH_2in plane bending	1450	1450	1457	1453	1439	1453	1455
CH_3bend	-	-	-	1376	1365	1378	1379
M-N	-	591	616	633	686	633	590
M-O	-	487	433	492	658	499	493

Table 2: FTIR of the Imine chelator, LH and its bivalent metal chelates

Electronic spectral, Molar Conductivity and Magnetic Moment measurements

The compounds' Uv-vis spectra revealed intra-chelator (n→π*, π→π*) and intra/inter chelates (d-d, L→MCT) transitions. The geometries of the chelates were assigned based on electronic absorptions and µ*eff* data (Festus et al., 2021; Nevin and Kenan, 2018). The ultraviolet spectra of the imine chelator showed five bands. The bands at 40222 and 33784 cm^{-1} were caused by charge transfer and π→π* transitions in the LH naphthalene unit (Ajlouni et al., 2012, Taha et al., 2012, Festus et al., 2021). The latter also appeared at lesser wavenumbers within the spectra of the bivalent chelates due to chelation of the LH with the M(II) ions. The bands assigned to intra-LH (π→π*) for $[Mn(L)_2(H_2O)_2]$, $[Fe(L)_2(H_2O)_2]$, $[Co(L)_2(H_2O)_2]$, $[Ni(L)_2](H_2O)$ and $[Cu(L)_2(H_2O)_2]$ chelates were observed at 39841 and 33898; 33784 and 33003; 39841; 39841 and 33784; and, 39683 and 33784 cm^{-1} correspondingly. Based on LH field transitions, the spectra of $[Fe(L)_2(H_2O)_2]$ and $[Zn(L)_2(H_2O)_2]$ chelates revealed additional low intensity bands in the visible area (Chioma, 2017b). The $[Mn(L)_2(H_2O)_2]$ chelate exhibited a band at 25000 cm^{-1} that might be attributed to a n→π* transition associated with imine moiety coupling (Gomathi and Selvameena, 2013). Other bands at 16611, 15674, and 14641 cm^{-1} were ascribed to $^6A_{1g}\rightarrow{}^4T_{1g}(G)$, $^6A_{1g}\rightarrow{}^4T_{1g}$, and $^6A_{1g}\rightarrow{}^4T_{2g}(G)$ transitions respectively typical of a 6-coordinate assemblage. Fe(II) chelates are found in coordination sites that are near to octahedral and tetrahedral symmetry (Cotton et al., 1999). The $[Fe(L)_2(H_2O)_2]$ chelate demonstrated a n→π* transition at 29851cm^{-1}, with large bands owing to Jahn Teller effects at 16077 and 14684cm^{-1} attributable to the $^5T_2g\rightarrow{}^5Eg$ transition and compatible with a 6-coordinate geometry (Chioma et al., 2023). High spin Co(II) chelates with $^4T_2(t_2^5e^2)$ and $^2E(t_2^6e^1)$ configurations frequently exhibit spin crossover equilibrium (Festus et al., 2021). Two absorption bands at 15625 and 14771 cm^{-1} in the visible spectra of the $[Co(L)_2(H_2O)_2$ chelate were identified and ascribed to $^4T_{1g}\rightarrow{}^4A_{2g}$ and $^4T_{1g}\rightarrow{}^4T_{1g}(P)$ transitions corresponding to a d^7 high spin octahedral system with 4^F ground term (Festus and Okocha, 2017). The assignment of high spin 6-coordinate assemblage to the latter was verified by the calculated µ*eff* of 4.9BM since µeff of Co(II) chelates were likely to be higher than the spin only value for 6-coordinate octahedral chelates due to orbital contributions (Nevin and Kenan, 2018, Festus, 2017). Two visible spectral bands at 15549-14706 cm^{-1} were ascribed to the $^3A_{2g}\rightarrow{}^3T_{1g}(F)$ transition by the Ni(II) chelate. An u*eff* of 4.0 BM found for the Ni(II) chelate clearly supported the attribution to tetrahedral assembly. Bivalent nickel chelates with tetrahedral structure are paramagnetic, with µ*eff* values ranging from 3.70 to 4.0BM (Munde et al., 2012). The spectra of Cu(II) chelate showed a wide band at 13123, 14728, and 15924 cm^{-1} ascribed to the $^2E_g\rightarrow{}^2T_{2g}$ transition induced by Jahn-Teller distortion 6-coordinate assemblage (Cotton et al., 1999). The absence of bands below 10,000 cm^{-1} ruled out a tetrahedral shape. The visible spectra of the Zn(II) chelate did not display any d-d transition band, which is typical with Zn(II) chelates. The chelates' molar conductivity values **(Table 1)** are in the range 9.3-37.2 $\Omega^{-1}cm^{-2}mol^{-1}$, indicating their non-electrolytic character.

COMPOUNDS	ABSORPTION	BAND ASSIGNMENT	GEOMETRY
LH	40323 33784 19531	**CT**	
$[Mn(L)_2(H_2O)_2]$	39841, 33898 25000 16611 15674 14641	π→π* n →π* $^6A_{Ig}\rightarrow{}^4T_{Ig}$ $^6A_{Ig}\rightarrow{}^4T_{Ig}$ $^6A_{Ig}\rightarrow{}^4T_{2g}$	Octahedral
$[Fe(L)_2(H_2O)_2]$	40161 33784, 33003 29,851 16,077 14,684	CTT π →π* n →π* $^5T_{2g}\rightarrow{}^5E_{Ig}$ $^4T_{2g}\rightarrow{}^5E_{Ig}$	Octahedral
$[Co(L)_2(H_2O)]$	39,841 15,625 14771	π→π* $^4T_{1g}\rightarrow{}^4A_{2g}$ $^4T_{1g}\rightarrow{}^4A_{2g}$	Octahedral
$[Ni(L)_2](H_2O)$	39841, 33784 15649 14706	π →π* $^3T_1\rightarrow{}^3T_I(F)$ $^2A_1\rightarrow{}^3T_1(F)$	Tetrahedral
$[Cu(L)_2(H_2O)_2]$	39683, 33784 15924 14728, 13123	π →π* $^2E_g\rightarrow{}^2T_{2g}$ $^2B_{1g}\rightarrow{}^2A_{1g}$	Octahedral
$[Zn(L)_2(H_2O)_2]$	40323 18416, 15456	M-LCT	Octahedral

Table 3: Electronic Absorption (cm^{-1}) Spectra data of the Compound

Biological Studies

Antibacterial Activities: Antibacterial activities of LH and its bivalent chelates were assessed on six microbial strains *S. aureus, E. coil, S. Epidermis, K. oxytoca, S. pneunoniea* and *P. mirabilis* via a disc diffusion method (Sharma et al, 2009). Streptomycin was utilized as positive control. The antibacterial results **(Table 4)** demonstrated that, with the exception of *P. mirabilis*, the tested chelates were active against the microorganisms. This might be related to the chelation effect, which boosts antibacterial activities principally due to the partial dispersion of oxidative charge resident on the M^{2+} with LH heteroatoms and possible electron delocalization on the cyclic rings (Atmaram et al., 2011; Chioma, 2017b). $Zn(L)_2(H_2O_2)$ chelates inhibited *S. pneumoniea* more effectively, with inhibitory zones of 9.0 and 15.0 mm, respectively. The chelator was exclusively effective against *K. oxytoca*. The Ni(II) plus Zn(II) chelates repressed *S. pneumoniea* more efficiently, with inhibitory zones of 9.0 and 15.0 mm, respectively. The sensitivity of Ni(II) and Zn(II) chelates could be attributed to bacterial organisms producing potent protein toxins to activate their cell surface proteins, preventing adequate permeation of the chelates into the bacteria cells, as well as lower lipophilicity of the chelates, which also reduces their penetration through the lipid cell membrane (Festus et al., 2021). The Mn(II) plus Ni(II) chelates remained inactive against all the microbes except *S. epidermidis*. $[Fe(L)_2(H_2O)_2]$

remained active against 4 organisms; *S. aureus, E. coil, K. oxytoca* and *S. pneumoniea* with inhibitory zones range of 4.0-7.0 mm. $[Co(L)_2H_2O_2]$ had a little antibacterial effect on *S. aureus* and *S. epidermidis* but had no effect on other bacterial species. Except for *S. pneumoniea*, which showed an inhibitory zone of 5.0 mm, the $[Cu(L)_2(H_2O]$ chelate had no effect against all bacteria species. The inhibitory zone of $Zn(L)_2(H_2O)_2$ against *S. pneumoniea* was 15.0 mm, which was more than the antibacterial medication employed. The superior antibacterial activity of the $Zn(L)_2(H_2O)_2$ complex over the comparable chelating drugs may be explained using the overtone idea and Tweedy's chelation theory (Festus et al., 2021).

According to the overtone notion of cell permeability, the hydrophobicity of the lipid membrane that surrounds the cell enables only lipid soluble molecules to pass through, which is a vital factor that affects anti-microbial action (Puja et al., 2016, Faraja et al., 2018). The polarity of the metal ion is greatly reduced during chelation due to chelator orbital overlap and partial sharing of the metal ion's positive charge with donor groups. Furthermore, it promotes the delocalization of elections across the whole chelate ring and increases the lipophilicity of the chelates (Ahmed et al., 2015). This enhanced lipophilicity facilitates the entry of chelates into lipid membranes, halting the numerous metabolic processes of microorganisms. The enhanced activity of chelates can be attributed to the presence of a M+ ion in normal cell activities (Chaturvedi, D., &Kamboj, M. 2016).

Antifungal Activity: The chelator and its M(II) chelates were further tested for anti-fungal activity against three fungal strains: *A. flavus*, *Fuserium sp*, and *A. niger*. The positive control was miconaozole. The antifungal results (Table 4) revealed that $[Mn(L)_2(H_2O)_2]$ had the most potent antifungal activity against *A. niger*. Antifungal activities revealed that the chelator had a lower inhibitory impact on the fungus with inhibition zones lower than its chelates. However, after coordination with metal ions, the latter's effects were more effective and prominent. This increase might be attributed to chelate toxicity, which is caused by a synergistic impact between the metal ion and the Lewis base. Other aspects that may have contributed to the chelates' improved antifungal activity include chelation and a greater steadiness constant. All The chelates displayed comparable inhibitory zones with *A. flavus* and *A. niger* to the conventional medication (El-Sherif et al., 2012; Chioma, 2017b). When compared to the usual medication, the bivalent chelates demonstrated more pronounced antifungal activity.

Compounds	Bacterial		Organisms		Fungal Organisms				
	S. aureus	***E. coli***	***S. epidermidis***	***K. oxytoca***	***S. pneumoniea***	***P. mirabilis***	***A. flavus***	***Fuserium Sp***	***A. niger***
LH	0.0±0.0	0.0±0.0	0.0±0.0	8.0±0.0	0.0±0.0	0.0±0.0	15.5±0.5	6.0±0.0	23.0±1.0
$[Mn(L)_2(H_2O)_2]$	.0±0.0	0.0±0.0	8.0±0.0	0.0±0.0	0.0±0.0	0.0±0.0	17.5±0.5	8.0±0.0	26.5±0.5
$[Fe(L)_2(H_2O)_2]$	6.5±0.0	4.0±0.0	0.0±0.0	6.5±0.0	6.0±0.0	0.0±0.0	21.0±1.0	21.0±1.0	20.5±0.5
$[Co(L)_2(H_2O)_2]$,	5.5±.5.0	0.0±0.0	8.0±0.0	0.0±0.0	0.0±0.0	0.0±0.0	13.0±1.0	0.0±0.0	26.0±0.0
$[Ni(L)_2]H_2O$	0.0±0.0	0.0±0.0	9.0±1.0	0.0±0.0	0.0±0.0	0.0±0.0	11.5±0.5	0.0±0.0	25.0±1.0
$[Cu(L)_2(H_2O)_2]$	0.0±0.0	0.0±0.0	0.0±0.0	0.0±0.0	4.5±0.5	0.0±0.0	12.0±0.0	14.5±0.5	26.0±0.0
$[Zn(L)_2(H_2O)_2]$	11.0±1.0	0.0±0.0	0.0±0.0	0.0±0.0	15.0±1	0.0±0.0	14.0±0.0	20.0±0.0	22.0±0.0
Streptomycin/ Miconazole	14.0±0.0	15.0±1.0	11.0±1	12.0±0	13.5±.5	9.0±1.0	8.0±0.0	0.0±0.0	10.0±0.0

TABLE 4: Anti-Bacteriological Actions of LH and its bivalent metal chelates

CI - DATA

Gravimetric Measurements: Gravimetric measurements of ms were performed at 303K in the absence and presence of 100-500 ppm uniform complex solution to investigate the influence of LH and its chelates on corrosion of ms in 1M HCl. As a control, a 100 ppm blank solution with no chemical was used. Table 5 and Figures 1(a) and (b) show the percentage (%) IE and CR determined from weight decreases over 5 hours. The research showed that LH and its chelates have significant CI potentials in comparison to ms corrosion in a 1M HCl solution. The better inhibitory result of LH might be attributed to chelation via the donor acceptor interaction between the undistributed electron pairs of LH donor atoms and metal ions (Jacob et al., 2010; Odozi et al., 2020). The chelates outperformed the uncoordinated LH in terms of IE. The latter may be attributable to the chelates' huge masses and molecular planarity. Table 6 summarizes the findings of CR, Θ, and IE from gravimetric assessment at different doses of the inhibitor(s) at constant temperature and different times. The research demonstrated that as concentrations increased, CR reduced. The drop is due to the inhibitor concentration's inhibitive impact. It was also discovered that as inhibitor concentration rose, IE increased, yielding values of 94.34%, 97.62%, 97.92%, 97.28%, 94.44%, and 93.22% for LH, Mn(II), Fe(II), Co(II), Ni(II), and Zn(II), respectively. This might be attributed to LH adsorption on the ms surface by bonding free electron pairs of N- and O-atoms, as well as -electrons of the cyclic rings combining with the imine moiety. The chelates were arranged as follows: Fe(II)>Mn(II)>Co(II)>Ni(II)>LH>Zn (II). This denoted that Fe(II) chelate had the greatest IE (97.92%), while Zn(II) chelate had the lowest (93.22%). The discrepancy in inhibitory performance was most likely due to differences in the chelates' stability and solubility in acid solution (Mahendra et al., 2012, Festus and Wodi 2021).

compound	CONC.	CR	% IE	Θ	ΔW
LH	BLANK	0.0053	-	-	0.0265
	100	0.0042	20.75	0.2075	0.0210
	200	0.0038	28.30	0.2830	0.0190
	300	0.0007	86.79	0.8679	0.0035
	400	0.0004	92.45	0.9245	0.0020
	500	0.0003	94.34	0.9434	0.0015
$[Mn(L)_2(H_2O)_2]$	BLANK	0.0042	-	-	0.0210
	100	0.0006	85.71	0.8571	0.0030
	200	0.0004	90.48	0.9048	0.0020
	300	0.0003	92.86	0.9286	0.0015

	400	0.0002	95.24	0.9524	0.0010
	500	0.0001	97.62	0.9762	0.0005
$[Fe(L)_2(H_2O)_2]$	BLANK	0.0060	-	-	0.0300
	100	0.0038	87.50	0.8750	0.0038
	200	0.0040	93.00	0.9300	0.0020
	300	0.0004	93.75	0.9375	0.0019
	400	0.0003	95.83	0.9583	0.0003
	500	0.0001	97.92	0.9792	0.0006
$[Co(L)_2(H_2O)_2]$	BLANK	0.0046	-	-	0.0231
	100	0.0010	78.26	0.7826	0.0050
	200	0.0006	86.41	0.8641	0.0031
	300	0.0004	91.85	0.9185	0.0018
	400	0.0003	94.57	0.9457	0.0013
	500	0.0001	97.28	0.9728	0.0006
$[Ni(L)_2(H_2O)]$	BLANK	0.0045	-	-	0.0225
	100	0.0020	55.56	0.5556	0.0100
	200	0.0008	83.33	0.8333	0.0038
	300	0.0005	88.89	0.8889	0.0025
	400	0.0004	91.67	0.9167	0.0018
	500	0.0003	94.44	0.9444	0.0013
$Zn(L)_2(2H_2O)$	BLANK	0.0059	-	-	0.0295
	100	0.0021	64.41	0.6441	0.0105
	200	0.0008	86.44	0.8644	0.0040
	300	0.0007	88.14	0.8814	0.0035
	400	0.0006	89.83	0.8983	0.0030
	500	0.0004	93.22	0.9322	0.0020

Table 5: The weight, % IE and CR obtained for a ms immersed in 1M HCl of the compounds at 303K for 5 hr

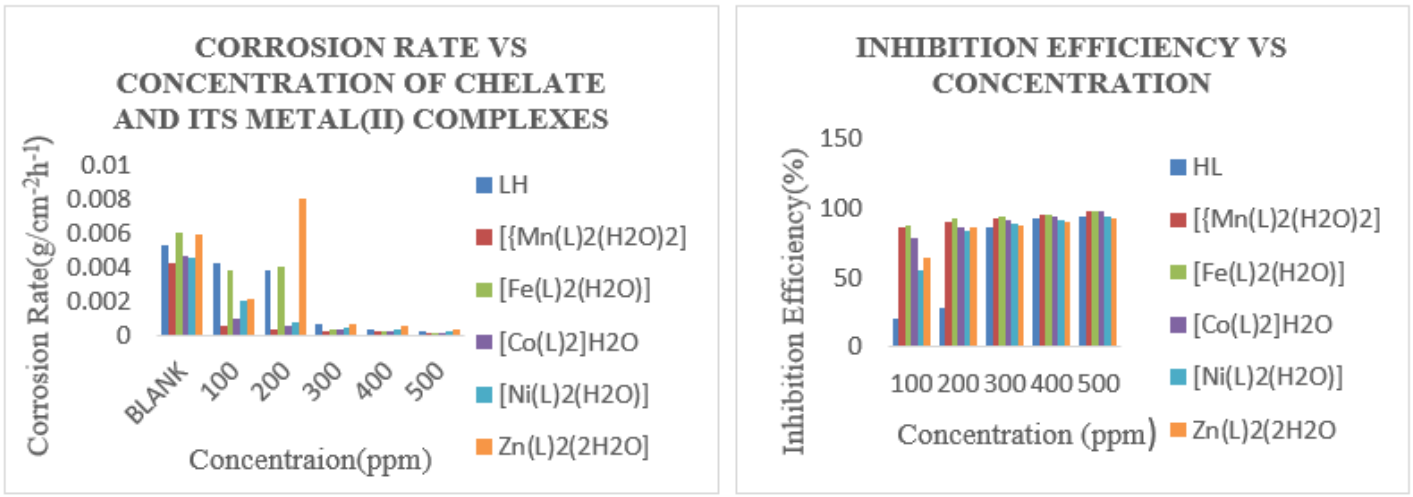

(a) **(b)**

Figure 1: variation of CR (a) and IE (b) against concentration of LH and its chelates at 303K

Quantum (Dft) Studies

Global Reactivity: The quantum chemical calculations and DFT methods adopted were as reported in literature (Chioma et al., 2022; Wodi et al., 2022). Figure 2 shows the optimized chemical structure of LH and its complexes. Figure 3 depicts the optimized HOMO and LUMO orbital structures for the compounds. As revealed in Table 6, the complexes studied, exhibited greater *E*HOMO data but lesser *E*LUMO data. Zn(II) complex had the highest *E*HOMO value (-5.288793 eV) whereas Fe(II) complex had least *E*HOMO value of -4.719804 eV. It is obvious that the HOMO level was located on both *N* plus *O* atoms; so these spots were preferred for the electrophilic evaluation on the metal exterior. Such justifications denote the capability of the chelates to be adsorbed on the metal exterior, therefore suggesting the anticorrosion potential, which conforms with the investigational results (Festus et al., 2020; Gouda et al., 2022). *E*HOMO is regularly connected with the strength of a molecule to give electron (Popova et al., 2003). Enhanced value of *E*HOMO matched to that of *E*LUMO connotes that the molecule is an electron giver to a appropriate electron acceptor possessing low unfilled molecular orbital. This high value boosts the adsorption that further impedes corrosion on the metal surface. *E*LUMO energy confirms the strength of a molecule to accept electron (Popova et al., 2003), and low data of *E*LUMO connotes that the molecule will possess improved potential electron acceptor. LH ligand had the lowest *E*LUMO with a value of -2.07323 eV, in agreement with experimental data.

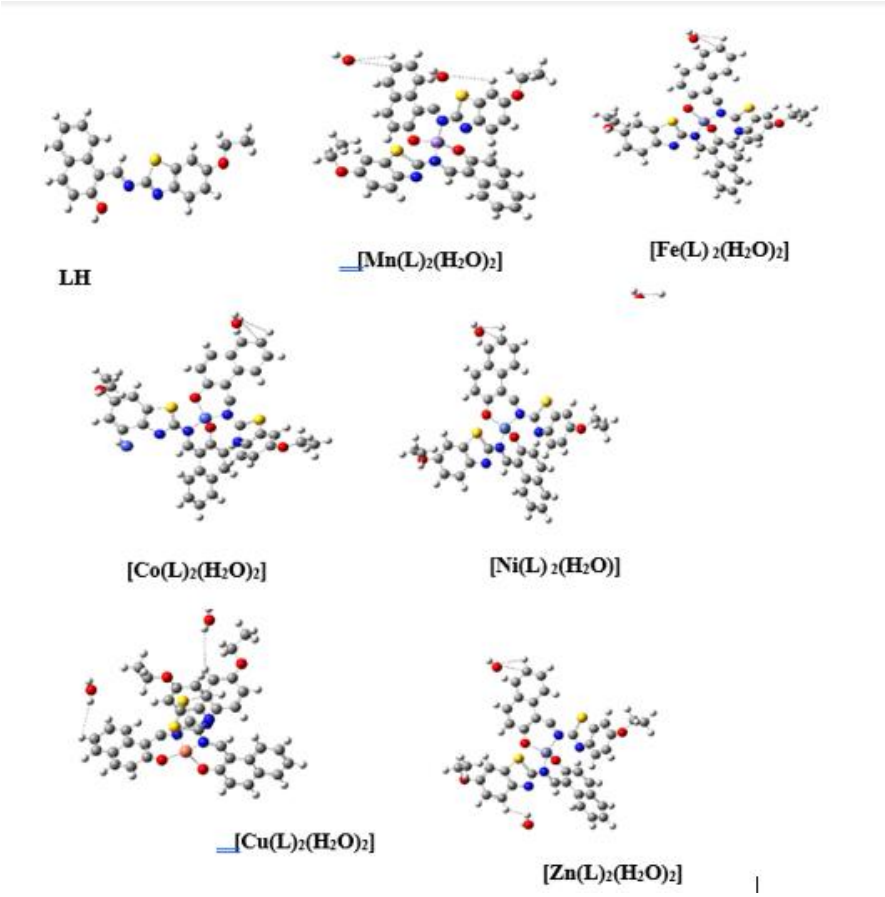

Figure 2: Optimized structures for LH and its complexes calculated by B3LYP/6-31G (d, p)

The low value of Δ*E*indicates a greater propensity of inhibitor to be adsorbed on the steels exterior (Festus et al., 2020, Abd El-Lateef et al., 2020). As verified in Table 6, all the complexes displayed low energy gap (*E*LUMO- *E*HOMO) indicating high reactivity. These Δ*E* values (3.20169-1.694721eV) designate a transfer of electron from HOMO to LUMO. This denotes that the complexes have excellent adsorption strength and can increase chemical reactions because they all have low energy gap values, with LH having the lowest tendency to accept an electron, indicating a lower tendency for electrons to move to the excited state when compared to its chelates. Because of its lower energy gap, the $[Cu(L)_2(H_2O)_2]$ complex showed a stronger inclination to donate electrons than others (1.694721 eV).

Parameters Inhibitors(eV)	HL	$[Mn(L)_2(H_2O)_2]$	$[Fe(L)_2(H_2O)_2]$	$[Co(L)_2(H_2O)_2]$	$[Ni(L)_2(H_2O)]$	$[Cu(L)_2(H_2O)_2]$	$Zn(L)_2 2H_2O$
E_{HOMO}	-5.27492	-4.904025	-4.719804	-5.169593	-5.19245851	-4.9862032	-5.288793
E_{LUMO}	-2.07323	-2.400311	-2.389971	-2.552694	-2.1603071	-3.29148187	-2.420447
Δ*E*	3.20169	2.503714	2.329833	2.616899	3.0321514	1.694721	2.867483
Ionization potential	5.27492	4.904025	4.719804	5.169593	5.192458508	4.9862032	5.288793
Electron Affinity	2.07323	2.400311	2.389971	2.552694	2.1603071	3.29148187	2.420447
Electronegativity χ	3.36741	3.652168	3.5548875	3.861144	3.6763828	4.1388425	3.854689
CH pot	-3.36741	-3.652168	-3.554888	-3.861144	-3.6763828	-4.1388425	-3.854689
Hardness η	1.600845	1.251857	1.1649165	1.308450	1.516075704	0.84736067	1.434173
Softness σ	0.624670	0.798813	0.8584306	0.764263	0.659597668	1.180135019	0.697266
Electrophilicity index ω	4.216168	5.327418	5.4240905	5.696983	4.45749195	10.10786661	5.180207
Chemical potential μ	3.716718	2.159003	4.123912	7.930256	4.813942	6.337552	6.745878

Table 6: Quantum Chemical Variables

The high χ values depict the potential of inhibitors to receive electrons, forming a strong bond with the metal atom (Abd El-Lateef et al., 2020), on the other hand, less χ data proves the capability of inhibitor molecules to give out electrons. Many inhibitors display averagely less χ data suggestive of their strength to give out electrons. Our acquired data (Table 7) depicts that the χ of all the compounds were very low indicative that they're all electron donors with $[Cu(L)_2(H_2O)_2]$ complex having the highest value of 4.1388425 eV and LH having the least value of 3.36741 eV (Upadhyay et al., 2021; Wodi et al., 2022). Often, compounds are evaluated for firmness plus susceptibility from its η or σ values. A soft molecule has a small energy gap while a hard molecule has a large energy gap (Spirtovic-Halilovic et al., 2014). In this current work, the compounds displayed low energy gaps, hence are soft molecules. They all show strong strength to inhibit electron transfer to the studied steel, giving rise to a strong anticorrosion potential.

To appraise the exclusion value of a compound, dipole moment (DM) is adopted (Oyebamiji & Adeleke 2018). Increase in DM produces corresponding a rise in the efficiency of the CI (Singh et al., 2020).

Looking through Table 6, the calculated DM reveal that all studied complexes except $[Mn(L)_2(H_2O)_2]$ (with low DM), possess the tendency to interact with high DM species such as biological systems due to high DM character (Chioma et al., 2023). The *A* disclosures an entire energy needed for a chelator to become electron acceptor whereas the *I* depicts the strength of a chelator to become an electron donor (Odozi et al., 2020; Gouda et al., 2022). The result obtained for *I* and *A* for the compounds studied depicts high figures of I and low figures for A corroborating the strength of the compounds both to give and receive electrons. The ω factor estimates chemical reactivity as it affords data on both η and μ of a compound. Higher data of ω were taken to depict a better electrophile while a lesser ω data denote nucleophilic strength (Gouda et al., 2022; Bououden et al., 2020; Diki et al., 2021). The low electrophilic values of Ψ = 4.216168eV (LH), Ψ =5.327418eV ($[Mn(L)_2(H_2O)_2]$), Ψ =5.4240905eV ($[Fe(L)_2(H_2O)_2]$), Ψ = 5.696983eV ($[Co(L)_2(H_2O)_2$], Ψ = 4.45749195 eV $[Ni(L)_2]H_2O$, Ψ = 10.10786661 eV $[Cu(L)_2(H_2O)_2]$ and Ψ = 5.180207 eV $Zn(L)_2(H_2O)_2]$ compounds shows they were good nucleophiles which indicates higher chemical reactivity.

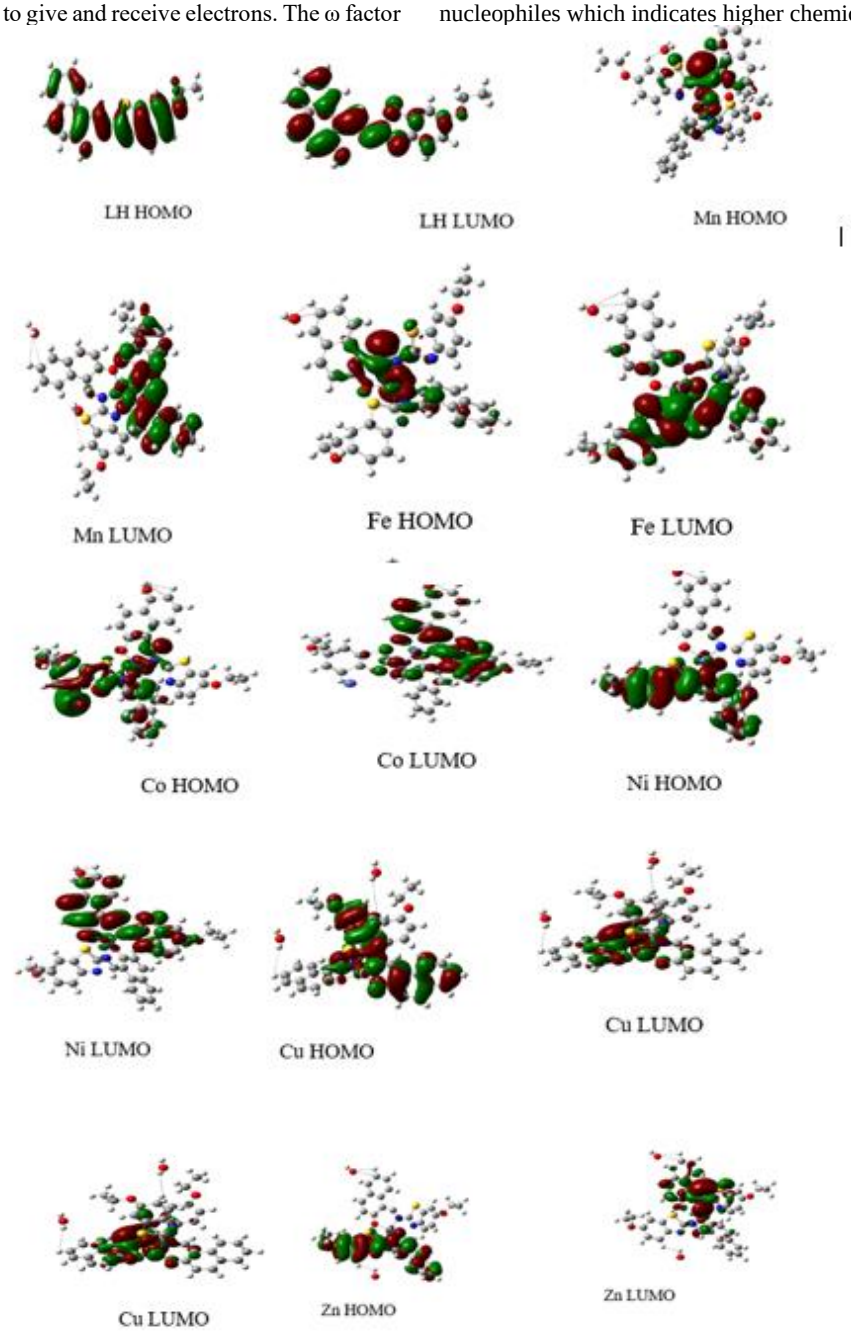

Figure 3: HOMO and LUMO diagrams of the chelator and its chelates by B3LYP/6-31G (d, p)

Conclusion

An imine chelator obtained from the condensation of 2-HNA and 2-AEBT as well as its bivalent chelates have been synthesized and characterized. Additionally, they were examined for biological and CI potentials. A 6-coordinate assemblage was assigned to the bivalent chelates on the basis of UV-vis and u_{eff}data except for Ni(II) chelate which adopted tetrahedral geometry. The low conductance data supported the fact that the chelates were non electrolytes. The imine chelator plus its chelates had myriad shades distinctive from their precursors. The FTIR spectrum of the chelator presented a band at 1622cm $^{-1}$that shifted to 1616-6220 cm^{-1} in the chelates, and was assigned to -C=N- moiety. This

present study showed that $[Zn(L)_2(H_2O)_2]$ had the highest antibacterial actions against Streptococcus *p.* The highest antifungal action was displayed against *A. niger* by $[Mn(L)_2(H_2O)_2]$ chelate (26.5mm). The effect of imine chelator on acid corrosion of ms could be evident from the result that the chelator showed considerable CI behavior in opposition to corrosion of ms in a 1M HCl solution. The absorption of the composite compounds on the metal surface which was proven by the Density Functional Theory calculations showed that the chelator and its chelates are potential corrosion inhibitors for steel protection.

References

1. Solution using Newly Uynthesized urea-Based Cationic Fluorosurfactants: Experimental and computational investigations. New Journal of Chemistry, 44,17791–17814.
2. Ahmed, M., Abu-Dief, Ibrahim, M.A. (2015). Areview on versatile applications of transition metal complexes incorporating Schiff bases. Beni-Suef University Journal of Basic and Applied Sciences, 4(2), 119- 133.
3. Ajlouni, A. M., Taha, Z.A., Al-Hassan, A.K, &Anzeh A.M.A.(2012). Synthesis, Characterization, luminescence properties and Antioxidant Activity of ln(III) chelates with a new aryl amide bridging ligand. Journal of luminescence, 132(6),1357- 1363,
4. Aliyu, H. N., & Sani, U. (2012). Synthesis, characterization and biological activity of Mn(II), Fe(II), Co(II), Ni(II), and Co(II). Schiff base chelates against multidrug resistant bacteria and fungi pathogens. International Research Journal of pharmacy and Pharmacology,2,40 - 44
5. Amani S. Alturiqi, Abdel-Nasser M.A. Alaghaz, Reda A. Ammar and Mohamed E. Zayed, (2018). Synthesis, Spectral Characterization, and Thermal and Cytotoxicity Studies of Cr(III), Ru(III), Mn(II), Co(II), Ni(II), Cu(II), and Zn(II) Complexes of Schiff Base Derived from 5-Hydroxymethylfuran-2-carbaldehyde. Journal of Chemistry, 17,
6. Abel-Olaka, L. C., Kpee, F. & Festus, C. (2019). Solvent Extraction of 3dMetallic Elements using N2O2Schiff Base-Chelators: Synthesis and Characterization. Nigerian Research Journal of Chemical Sciences. http://www.unn.edu.ng/nigerian-research-journal-of-chemical-sciences/
7. Atmaram, K.M.and Kirian. V.M (2011). Synthesis, Characterization and Antimicrobial Activity of Mixed Schiff Base Ligand Complexes of Transition Metal(II) Ions. International Journal of ChemTech. Research., 3(1):477- 482
8. Sadi, A. H., Idris, M.I and Bashir, S.S. (2006). Synthesis, Characterization and Antimicrobial Studies of Ru(II) Complexes with Schiff Base co-ligand derived from 5,6-diamino-1,10-phenanthroline and benzene-1,4-dicarbaldehyde. Bayero Journal of Pure and Applied Sciences. 10(1):468-476
9. Bououden, Walid, &Benguerba,Yacine (2020). Designing, Cytotoxic Evaluation, moleculara Docking and in Silico pharmacokinetic prediction of New Hydrocortisone Derivatives as anti asthmatics drugs. Journal of Drug Delivery and Therapeutics.10(4), 8-16.
10. Chaturvedi, D., & Kamboj, M. (2016). Role of Schiff Base in Drug Discovery Research. Chemical. Science Journal:e114.7:2.
11. Chioma F., Ima-Bright N. and Osi, V. (2022). Synthesis; Spectral, Computational Studies; and Antimicrobial Evaluations of Fe(II) and Zn(II) chelates containing RC-NR and N2O 2 moieties, J. Anal Pharm Res., 11(2):45–54. 10.15406/japlr.2022.11.00401
12. Cotton, F. A., Wikinson, G., Murillo, C.A., & Bochmann, M.(1999). Advance inorganic chemistry, 6thed. John Wilel,New York
13. Chioma, F. (2017b). Synthesis, Characterization and Antibacterial Studies of Heteroleptic Co(II), Ni(II), Cu(II) and Zn(II) Complexes of N-(2-hydroxybenzylidene)pyrazine-2-carboxamide. International Journal of Chemistry, Pharmacy &Technology, 2(5); 202-211
14. Chioma, F., Chizoba, I. E. & Obinna, O. (2023). Synthesis, characterization, DFT and Biological Studies of Fe(II), Cu(II), and Zn(II) complexes of keto-imine Chelators. Inorganica Chimica Acta, 545 (2023) 121255
15. Chioma F. and W. C Theresa. (2022). Novel M2+ Complexes of 2-(thiazole-2-ylamino)-2,3-dihydonaphthalene-1-4-dioneschiff base: Design, preparation, characterization and corrosion inhibition studies. Journal of Applied Sciences, 22:152 – 165,
16. Diki, N.Y.S., Coulibaly, N.H., Kambiré, O. and Trokourey, A.(2021). Experimental and Theoretical Investigations on Copper Corrosion Inhibition by Cefixime Drug in 1M HNO3 Solution. Journal of Materials Science and Chemical Engineering, 9, 11-28.
17. Debdulal, M. (2019). Biological Applications of Schiff baseMetal Complexes- A Review. International Journal of Research and Analytical Review. 6(2, 471-477,
18. El-Sherif, A.A, Shoukry, M.M and Abd-Elgawad, M. M. (2012). Synthesis, Characterization, Biological Activity and Equilibrium Studies of Metal(II) Ion Complexes with Tridentate Hydrazine. Spectrochemica Acta part A. Molecular and Biomolecular Spectroscopy, 98, 307-321. Doi:10.1016/j.saa.2012.08.034
19. Faraja , D. ., Jihen, L., Wenhua, M., Jinhu, X., Fedrick, C., Meiling, C., and Shaim. (2018). Antimicrobial Properties and Mechanism ofAction of some plant Extract AGAINST food Pathogens and Spoilae Microorganisms. food Microbiology, 9.
20. Fayomi, S.O., Olusanyan, D., Ademuyiwa, F.T., Olarewaju, G.(2021). Progresses on mild steel protection toward surface service performance in structural industrial:An overview, conference series: Materials Science and Engineering, 1036
21. Festus, C., Ekpete, O. A. and Don-Lawson, C. D. (2020). Novel metal2+ Complexes of N-(1,4-dihydro-1,4-oxonaphthalen-3-yl) pyrazine-2-carboxamide: Synthesis, Structural Characterization, Magnetic Properties and Antimicrobial Activities. Current Research in Chemistry, 12: 1-10
22. Festus Chioma. (2017). Synthesis, Experimental Characterization; and Antimicrobial, and Antioxidant Studies of some M2+Chelates of Schiff Base Ligand Bearing hydroxypyridine Moiety. Scholarly Journal of Scientific Research and Essay, 6(6), 174-180
23. Festus, C., Jude, I. A., Collins, U. I. (2021). Ligation Actions of 2-(3-hydroxypyridin-2-ylamino)naphthalen-1,4- dione: Synthesis, Characterization, In-vitro Antimicrobial Screening, and Computational Studies. Indian Journal of Heterocyclic Chemistry, 31(01); 1-13,
24. Festus C. & Okocha O. (2017). Behaviour of N-(2-hydroxybenzylidene)pyrazine-2-carboxamide in complexation towards Fe(II), Co(II), Ni(II) and Cu(II) ions: synthesis, spectral characterization, magnetic and antimicrobial properties. Int.l J. of Chem., Pharm. &Techn., 2(4); 143-153
25. Festus, C., & Wodi, C. T. (2021). Corrosion Inhibition; and Antimicrobial Studies of Bivalent Complexes of 1-(((5-ethoxybenzo[d]thiazol-2-yl)Imino)methyl)naphthalene-2-ol

Chelator: Design, Synthesis, and Experimental Characterizations. Direct Research Journal of Chemistry and Materials Science, 8(2021); 31-43

26. Festus, C., Don-Lawson, C. D. (2018). Synthesis, spectral, magnetic and in-vitro biological studies of organic ligands and their corresponding heteroleptic divalent d-metal complexes. The Pharmaceutical and Chemical Journal; 5(3):118-129.
27. Festus, C.,Odozi, W. N., and Olakunle, M. (2020).Preparation, spectral characterization and corrosion inhibition studies of (e)-n-{(thiophene-2-yl)methylene}pyrazine-2-carboxamide Schiff base ligand. Protection of Metals and Physical Chemistry of Surfaces, 56(3); 651–662,
28. Franceso, T., Fiorenzo, R., Giuliano, B., Cristina, B. & Anna Moresco.(1994).Synthesis and Characterization of Neutral Technetium(III) Complexes with Mixed S, P Bidentate Phosphine-Thiolate ligands. Crystal structure of Tc(SCH2CH2PPh)2(SCH2CH2PPh2O)] journal of the chemical society, Dalton Transaction, 1453- 1461
29. Fengtao Yu, Zhiqiang Wang, Shicong Zhang, Haonan Ye, Kangyi Kong, Xueqing Gong, Jianili Hua, He Tian. (2018). Molecular Engineering of Donor-Acceptor Conjugated Polymer/g- C3N44Heterostructures for significantly Enhanced Hydrogen Evolution Under Visible- Light Irradiation. Advanced Functional Materials, , 28,1804512,
30. Gomathi V. & Selvameena R. (2013). Synthesis, Spectroscopic, Electrochemical and Biological Studies of Novel Schiff Base Chelates derived from 4-(3–ethoxy–2–hydroxybenzylideneamino)–n–(Pyridin-2-yl) benezenesulfornamide. Main Group Chemistry, 12, 275 – 284
31. Gouda, M., Khalaf, M. M., Shalabi, K., Al-Omair, M.A., & El-Lateef, H.M.A. (2022). Synthesis and Characterization of Zn–Organic Frameworks Containing Chitosan as a Low-Cost Inhibitor for Sulfuric-Acid-Induced Steel Corrosion: Practical and Computational Exploration.. Polymers, 14, 228.
32. Iswatun, H.A., and Nurziana, N. (2021). A Brief Review on the Thiazole Derivatives: Synthesis, Methods and Biological Activities. Malaysian Journal of Analytical Sciences. 25(2):257-267
33. Jacob K.S & Parameswaran G.,(2010). Corrosion Inhibition of Mild Steel in HCl Solution by Schiff Base Furoin thiosemicarbazone. International Journal of ChemTech Research, 52, 224-228.
34. Jones, J. S., Francois, P Gabbai (2016). Coordination and Redox-Noninnocent Behavior of Ambiphilic Ligands Containing Antimony. Accounts of Chemical Research, 49(5), 857-867
35. Kpee, F., Ukachukwu C. V. & Festus C. (2018). Synthesis, Characterization and Extractive Potentials of Aminopyrimidine Schiff Base Ligands on Divalent Metal Ions. Nigerian Research Journal of Chemical Sciences.4(2); 193-203
36. Linda, R. A., Ahmad, K. A., Faris, T. A. (2021). Synthesis and Medicinal Attributes of Thiazole Derivatives: A Review. Systematic Reviews Pharmacy, 12(1): 290- 295
37. Meshah, M., Douadi, T., Sahli, F., Issaadi, S., Boukazoula, S., & Chafaa, S., (2018). Synthesis, Characterization, Spectroscopic Studies and Antimicrobial Act of Three New Schiff Bases Derived from Heterocyclic moiety. Journal of Molecular Structure, 1151, 41 - 48
38. Mohamed, F.E., Bdreidin, M. A., and Mohamed, F. F.(2021). An Overview on Synthetic 2-Aminothiazole-Based Compounds Associated with Four Biological Activities. Molecules, 26(5)1449
39. Madueke Nancy Ada, & Iroha Nkem. B.(2018). Protecting Aluminium Alloy of Type AA8011 From Acid Corrosion using Extract from Allamanda cathartica leaves International Journal of Innovative Research in Science, Engineering and Technology. 2018, 7, (10), 10251
40. Munde, V. A., Shelke, S. M., Jadhow, A. S., Kirdant, S. R., Vaidya, S. E., Shankarwar & Chondhckar, T. K. Adv. Appl. Sci. Res, 3 (2012) 175.
41. Mahendra Y., (2012). Synthesis, Characterization and Biological Activity of Some Transition Metal Complexes of N-Benzoyl-N-Z-thiophene thiocarbohydrazide. International Journal of Inorganic Chemistry, (8),
42. Nevin, T., &Kenan, B.,(2018). Synthesis., characterization and antioxidant activity of schiff base and its metal chelates. European Journal of Chemistry, 22-29, Doi:10.5155/eurjchem.9.1.22-29.1671
43. Nevin, T., &Kenan, B., (2018). Synthesis., characterization and antioxidant activity of schiff base and its metal chelates. European Journal of Chemistry,22-29.doi:10.5155/eurjchem.9.1.22-29.1671
44. https://fjs.fudutsinma.edu.ng/index.php/fjs/article/view/718
45. Oyebamiji, A.K.; Adeleke, B.B. (2018). Quantum chemical studies on inhibition activities of 2,3-dihydroxypropyl-sulfanyl derivative on carbon steel in acidic media. International Journal of Corrosion and Scale Inhibition. 7, 498– 508. Doi:10.17675/2305-6894-2018-7-4-2
46. Prakash S. (2019). Schiff bases: An overview of their corrosion inhibition activity in acid media against mild steel. Chemical Engineering Communications, 207(7), 985-1029,
47. Puja, L., Mohanty, A.K., Pankai, J., & Anita K. G. (2016). Contribution of Cell Surface Hydrophobicity in the Resistance of Staphylococcus aureus against Anntimicrobial Agents. Biochemistry Research International, 2016: 5
48. Popova, A., Christov, M. & Deligeorgiev, T. (2003). Influence of the Molecular Structure on the Inhibitor Properties of Benzimidazole Derivatives on Mild Steel Corrosion in 1 M Hydrochloric Acid. Corrosion, 59, 756-764.
49. Spirtovic-Halilovic S, Salilovic, M, Dzudzevic-Cancar, H, Trifunovic, S, Roca, S, Softic D &Zavrsnik, D (2014). DFT study and microbiology of some coumarin-based compounds containing a chalcone moiety. Journal of the Serbian chemical society, 79,436-443. 102298/jsc1306280775
50. Sharma, K, Agawal, S Gupta S.(2009). Antifungal, antibacterial and antifertility of biologically active macrocyclic chelates of tin(ii) . International Journal of chemistry, Tech Rex 2013 5, 456-463.
51. https://biointerfaceresearch.com/wp-content/uploads/2020/06/20695837106.69366963.pdf
52. Sahar F. Abbasi, Jummbad H. Tomma Emad T. Ali, (2021). Synthesis and Chariterization of New Schiff Bases and their 1,3-Oxazepines Derived from Phthalic Anhydride. Systematic Review in Pharmacy. 12(2);260-265
53. Sadia, A. D., Farhana A., Md. Saddam, H., Md Nuruzzaman, K., Zakaria, Choudhury, M. Z., Md. Kudrat, E., & Md. Mahasin A. (2018). A Short Review on Chemistry of Schiff Base Metal Complexes and their Catalytic Application. International Journal of Chemical Studies, 6(3): 2859- 2866
54. Singh, A., Ansari, K. R, Quraishi, M.A, & Kaya, S. (2020). Theoretically and experimentally exploring the Corrosion inhibition of N80 steel by pyrazol derivatives in simulated acidizing environment. Journal of Molecular Structure, 1206

55. Taha, Z.A., &Ajilouni A.M.,(2012). Synthesis, characterization, luminescence properties and antioxidant activity of mn(III) Chelates with a new Aryl Amide Bridging Ligand. J. of Luminescence, 132(6), 1357- 1363
56. Thakar,A. S., Pandya,K. S., Joshi,K. T., Panchol,A. M., (2011).). Synthesis, Characterization and Antibacterial Activity of Schiff Bases and their Metal complexes Derived from 4-Acyl-1-phenyl-3-methyl-2-pyrazolin-5-ones and 2-Amino-4(4-methylphenyl)-thiozole. Journal of Chemistry, 8(4), 1556-1565I
57. Upadhyay, A.; Purohit, A.K.; Mahakur, G.; Dash, S.; Kar, P.K. Verification of corrosion inhibition of Mild steel by some 4-Aminoantipyrine-based Schiff bases—Impact of adsorbate substituent and cross-conjugation. Journal of Molecular Liquid, 2021, 333, 115960.
58. Wodi, T. C., Festus, C. and E. Nlemonwu, (2022). Anticorrosive Potentials of nNphthoquinone/naphtha-aldehyde Schiff bases for Mild Steel in HCl Medium: Synthesis, Characterization, and DFT Studies, Journal of Chemical Society of Nigeria, 47(5)1075-1098.
59. Xavier, A., Srividhya, N. (2014). Synthesis and Study of Schiff base Ligands. IOSR Journal of Applied Chemistry, 7(11), 06-15
60. Zhaohua Huang, Genjin Yang, Zhaoliang Lin, and Junlian Huang. (2001). 2-[N 1-2-Pyrimidyl-aminobenzenesulfonamido] ethyl 4-bis (2-chloroethyl)aminophenylbutyrate: A potent antitumor agent. Bioorganic & medicinal chemistry letters, 11(9), 1099-1103.